

GNSS Jammer and Spoofer Mitigation via Multi-Antenna Processing

Jonas Elmiger, Gian Marti, and Christoph Studer

Abstract—Modern positioning relies on radio signals from global navigation satellite systems (GNSS). Their low receive power renders these radio signals susceptible to jamming attacks, in which malicious transmitters emit strong interference to disrupt signal acquisition. Moreover, GNSS are vulnerable to spoofing attacks, in which malicious transmitters mimic legitimate satellites by transmitting spurious GNSS signals.

We propose SCHIEBER, a novel method for multi-antenna GNSS receivers that mitigates jammers as well as spoofers without requiring any prior knowledge of the receiver position or attack type: Jammers are mitigated during signal acquisition using a recently developed adaptive spatial filtering technique. Spoofers are identified and rejected after signal acquisition using a novel approach that tests the consistency of acquired signals by comparing their respective direction of arrival (DoA) and pseudorange estimates in a test that is invariant with respect to the unknown receiver position. We demonstrate the efficacy of our method using extensive simulations of a GPS L1 C/A system under spoofing and jamming attacks.

Index Terms—GNSS, jammer mitigation, multi-antenna, positioning, spoofer mitigation

I. INTRODUCTION

POSITIONING through GNSS signals has become a vital component in countless technologies and applications of modern life [1]. Owing to the importance of GNSS technology, numerous state actors maintain their own constellations of navigation satellites. Due to the large orbital distance of these satellites, their signals arrive with significant attenuation at potential receivers. The low receive power of these signals and the fact that GNSS operate outdoors renders them vulnerable to hostile interference. In particular, GNSS are exposed to *jamming attacks*, in which malicious transmitters try to drown GNSS signals in noise to disrupt signal acquisition at the receiver. Moreover, since civil GNSS use direct-sequence spread spectrum (DSSS) coding [2] with publicly known spreading codes, they are also vulnerable to *spoofing attacks*, in which malicious transmitters mimic legitimate satellites by emitting spurious signals that are encoded with valid GNSS spreading codes. Such spoofing can take various forms [3]: While simple spoofing attacks cause the receiver to fail in correctly positioning itself, more sophisticated attacks such as replaying or meaconing [4] can take over the estimated position and steer it away from the true location. The use of encrypted spreading codes can alleviate the risk of spoofing but necessitates key confidentiality and is typically only used in military signals. A possible defense mechanism against the

spoofing of civil signals is message integrity protection as implemented by Galileo Open Service Navigation Message Authentication (OS-NMA) [5], [6]. OS-NMA authenticates transmission data based on early message signing with delayed key disclosure. In itself, however, it only permits detection—not mitigation—of spoofing attacks.

Multi-antenna receivers have the ability to spatially resolve signals, which allows them to (i) distinguish between signals from different origins and (ii) use spatial filtering for nulling signals from certain directions—this makes multi-antenna processing a promising basis for jammer and spoofer mitigation.

A. Contributions

We propose SCHIEBER, a novel method for jammer and spoofer mitigation in multi-antenna GNSS receivers. SCHIEBER can mitigate simultaneous attacks by multiple jammers and spoofers without requiring encrypted spreading codes and without requiring any *a priori* estimate of the receiver position. All that is required is a local almanac of current satellite positions as well as a rough estimate of the time, so that the receiver can autonomously infer the current positions of the GNSS satellites. SCHIEBER mitigates jammers during signal acquisition while spoofers are mitigated between pseudorange estimation and positioning.

For signal acquisition, SCHIEBER builds on a recently developed method for jammer-resilient synchronization [7], which uses adaptive spatial filtering for mitigating signals that interfere with the synchronization (or spreading) code. This enables SCHIEBER to acquire satellite signals even under strong multi-antenna jamming while simultaneously maintaining the basic principles of regular GNSS signal acquisition. Since the signal acquisition stage does not distinguish between spoofers and legitimate satellites, spoofed signals are identified and rejected in a second stage. To this end, SCHIEBER uses a novel approach in which it tests the consistency of *pairs* of acquired signals by comparing their respective directions of arrival (DoAs) and pseudorange estimates in a test that is invariant with respect to the unknown receiver position. The DoAs themselves are estimated using a modified version of the multiple signal classification (MUSIC) [8] algorithm that takes into account the spatial filter from the jammer-mitigating signal acquisition stage. Finally, to increase the robustness in case that a spoofed signal has slipped through the spoofer rejection stage, SCHIEBER uses an outlier-robust iteratively reweighted least squares (IRLS) approach to estimate the position based on those pseudoranges that were not rejected. We demonstrate the efficacy of SCHIEBER through extensive simulations of a Global Positioning System (GPS) L1 C/A system [9] under various spoofing and jamming attacks.

The authors are with the Dept. of Information Technology and Electrical Engineering, ETH Zurich, Switzerland. (email: joelmiger@student.ethz.ch, marti@iis.ee.ethz.ch, studer@ethz.ch)

The work of CS and GM was funded in part by an ETH Grant.

Our approach aspires to refrain from making unreasonable assumptions about the attackers. In particular, we do not assume that the number of jammers or spoofers is known, and we do not make assumptions on the strength of their signals, nor about how many satellites a single spoofer spoofs simultaneously.

B. Related Work

Through its use of DSSS, GNSS is inherently designed to be robust to interference [10]. Moreover, time-frequency filtering can further improve the resilience against interference with little additional effort [11]. However, such mitigation techniques are effective mainly against narrowband jammers. The same holds true for the adaptive notch filtering techniques proposed by [12]. However, while these methods are easy to integrate into traditional single-antenna receivers, they are ineffective against strong wideband jamming attacks [13]. One possibility for mitigating such attacks is given by multi-antenna receivers, which can block hostile interference through spatial filtering (also known as beamforming): Reference [14] leverages the beamforming capabilities of multi-antenna receivers by exploiting the spreading code repetitions in GPS L1 C/A, which are used to form beams towards legitimate satellites. However, the assumption of perfect Doppler tracking limits this method to a single legitimate signal. Alternatively, the method from [13] minimizes the power after the spatial filter under the assumption that the strongest signal directions correspond to jamming and/or noise. Similarly, the method from [15] treats the leading eigenvectors of the receive signal's spatial covariance matrix as estimates of the jamming signal, which are then null-steered. A main drawback of such techniques is that they require assumptions about how many interference dimensions need to be nulled (i.e., how many jammers are jamming), and that they can fail when that assumption is violated. Moreover, such methods fail against interference that mimics legitimate satellite signals, i.e., against spoofing.

Spoofing mitigation is often performed via completely different methods than jammer mitigation. The commonly implemented receiver autonomous integrity monitoring (RAIM) and Advanced RAIM [16] methods exploit the redundancy when receiving five or more satellites to find outliers among the signals. While these methods can detect spoofing events caused by single spoofers, they are (i) designed mainly to ensure satellite integrity and (ii) are vulnerable to spoofing through multiple spoofers. A method for general spoofing detection with single-antenna receivers is proposed in [17], where a takeover attack that aims to influence the derived position is assumed. Using a correct initial position in combination with tracking, their approach raises a spoofing alarm upon detecting multiple peaks during the acquisition of a single satellite spreading code. In similar fashion, reference [18] proposes to identify spoofing by noticing when a single satellite spreading code leads to multiple acquired signals, and to reject the signals that were acquired earlier (based on an assumption that spoofed signals will be acquired first because the spoofer signal is assumed to be stronger than the legitimate signal). Another alternative is described in [19], where the assumption of a straight-line receiver trajectory is used. This approach enables one to examine changes in signal Doppler and phase, which

must be different between signals that originate from different signal sources. If a single spoofer spoofs multiple signals, it can be detected this way. Just as for jammer mitigation, the spatial resolution capabilities of multi-antenna receivers are also useful for spoofer mitigation. Methods for multi-antenna spoofing detection are proposed in [20] and [21], which exploit that dual-antenna spatial diversity must create varying carrier-phase differences among legitimate signals. Since these characteristics are dependent on the receive DoA, an attacker cannot replicate the diversity characteristics when spoofing multiple satellite signals simultaneously from the same direction. The same assumption (of a single attacker antenna spoofing multiple satellite signals) is used in [22], which detects spoofing and estimates its DoA using a coprime-array. Direct DoA examination is performed in [23], where subsets of the measured DoAs are iteratively used to estimate the receiver's attitude and evaluated for compatibility with the expected DoAs. While this approach is not dependent on an assumption that a single spoofer spoofs multiple satellites, its computational complexity increases exponentially with the number of acquired signals. Reference [24] similarly suggests a DoA examination approach that compares DoA measurements against the almanac information. The considered distributed sensor array consists of an aircraft fleet with single-antenna receivers, which estimates the directions from signal arrival time differences. The required assumptions of perfectly synchronized clocks among receivers and precise awareness of their relative positions to each other are optimistic, which speaks in favor a multi-antenna single-platform approach.

Combined jamming and spoofing mitigation is demonstrated in [25], [26], which extract the jamming subspace from the incoming signal's spatial covariance matrix by assuming that the jamming and noise components dominate, and then project the signal into the orthogonal complement space. Their accompanying spoofing suppression is again based on an assumption that a single attacker imitates multiple signals simultaneously from the same direction. This allows the elimination of the strongest spatial direction once it crosses a spoofing detection threshold. Reference [27] presents the same jamming suppression approach and likewise assumes a single-antenna multi-satellite spoofer, but explicitly estimates DoA angles to eliminate signal directions appearing more than once. A similar combined approach is explained in [28], where the same jamming elimination projection is applied, but where another orthogonal projection in each signal tracking stage is added. This latter projection matrix is estimated via an antenna array orientation estimation, which is tracked by a Kalman filter and which allows conflicting signal directions to be found. This approach requires a rough initial position estimate to determine the true satellite DoAs.

In summary, while separate jammer and spoofer mitigation strategies can often be combined, only few works explicitly demonstrate the simultaneous efficacy of both. Moreover, many mitigation approaches are dependent on specific assumptions about the attackers (such as that the number of jammers is known, that a single spoofer spoofs multiple satellites simultaneously, or that the jammers or spoofer signals are much stronger than legitimate satellite signals), or they depend on an assumption that the receiver approximately knows its position

already from the beginning. In contrast to our method, none of these previous works present a feasible approach for positioning under both multi-antenna jamming and multi-antenna spoofing *without* any prior position information.

C. Notation

We use boldface lowercase and uppercase letters to denote column vectors $\mathbf{a} = [a_1, \dots, a_n]^T = [a_1; \dots; a_n] \in \mathbb{C}^n$ and matrices $\mathbf{A} = [\mathbf{a}_1, \dots, \mathbf{a}_m] \in \mathbb{C}^{n \times m}$, respectively. Complex conjugation, transposition, conjugate transposition, and Moore-Penrose pseudo-inversion are denoted as \mathbf{A}^* , \mathbf{A}^T , \mathbf{A}^H , and \mathbf{A}^\dagger , respectively. The Hadamard product of \mathbf{A} and \mathbf{B} is denoted $\mathbf{A} \odot \mathbf{B}$. The Euclidean norm of \mathbf{a} is $\|\mathbf{a}\|_2$, and the Frobenius norm of \mathbf{A} is $\|\mathbf{A}\|_F$. The $n \times n$ identity matrix is \mathbf{I}_n , and the all-zero vector is $\mathbf{0}_n \in \mathbb{C}^n$ (depending on the context, the subscript n indicating the dimension may be omitted). The cardinality of a set \mathcal{A} is $|\mathcal{A}|$, the largest integer smaller than or equal to x is $\lfloor x \rfloor$, and the distribution of a circularly symmetric complex Gaussian random vector with covariance matrix \mathbf{C} is $\mathcal{CN}(\mathbf{0}, \mathbf{C})$. Estimates are usually marked by a hat (e.g., \hat{x} is an estimate of x), and values that are iteratively updated are marked by a bracketed superscript (e.g., $x^{(k)}$, where k is the iteration index).

II. MODEL AND PREREQUISITES

A. Signal Model

We consider a stationary receiver equipped with B antennas located at some (unknown) position $\mathbf{o} = [x, y, z]^T$ (expressed in Earth-centered, Earth-fixed (ECEF) coordinates), and a satellite constellation consisting of S active satellites with instantaneous positions $\mathbf{o}_\zeta, \zeta = 1, \dots, S$. We assume a so-called *warm start* [16], which means that the receiver knows the instantaneous time (up to an unknown internal clock offset δt) and possesses an almanac of the satellite trajectories, so that it can infer the instantaneous positions \mathbf{o}_ζ of all satellites $\zeta = 1, \dots, S$.

The baseband receive signal at sample index k under the impact of $I_J \geq 0$ stationary single-antenna jammers and $I_M \geq 0$ stationary single-antenna spoofers is modeled as

$$\begin{aligned} \mathbf{y}[k] = & \sum_{\zeta=1}^S \mathbf{h}_\zeta[k] t_\zeta \left[k - \left\lfloor \frac{\Delta t_\zeta}{T} \right\rfloor \right] \\ & + \sum_{j=1}^{I_J} \mathbf{j}_j w_j \left[k - \left\lfloor \frac{\Delta t_j}{T} \right\rfloor \right] \\ & + \sum_{m=1}^{I_M} \mathbf{q}_m \tilde{t}_m \left[k - \left\lfloor \frac{\Delta t_m}{T} \right\rfloor \right] + \mathbf{n}[k], \end{aligned} \quad (1)$$

where $\mathbf{h}_\zeta[\cdot] \in \mathbb{C}^B$ is the channel from the ζ th satellite to the receiver, $t_\zeta[\cdot] \in \mathbb{C}$ is the ζ th satellite's transmit signal, Δt_ζ is the signal delay between the ζ th satellite and the receiver, and T is the sampling period. Similarly, $\mathbf{j}_j \in \mathbb{C}^B$ and $\mathbf{q}_m \in \mathbb{C}^B$ are the channels of the j th jammer and the m th spoofer, respectively; $w_j[\cdot]$ and $\tilde{t}_m[\cdot]$ are their respective transmit signals; and Δt_j and Δt_m are their respective path delays. Finally, $\mathbf{n}[k] \sim \mathcal{CN}(\mathbf{0}, \sigma_n^2 \mathbf{I}_B)$ is additive white Gaussian noise (AWGN).

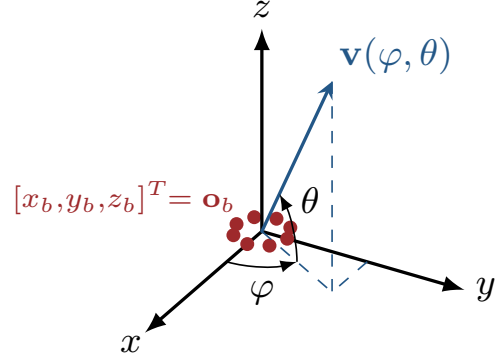


Fig. 1. Illustration of a unit vector $\mathbf{v}(\varphi, \theta)$ in a receiver-centric coordinate system with $B = 8$ receive antennas that are arranged in a ring in the xy -plane (with the b th antenna located at cartesian coordinates $\mathbf{o}_b = [x_b, y_b, z_b]^T$).

We assume that the channels between the satellites and the receiver are line of sight (LoS) with negligible multipath. Hence, the channel from the ζ th satellite to the receiver at sample index k can be expressed as

$$\mathbf{h}_\zeta[k] = \alpha_\zeta e^{i2\pi f_\zeta k T} \mathbf{a}_\zeta, \quad (2)$$

where $\alpha_\zeta \in \mathbb{C}$ is the distance-induced complex attenuation, which is equal to zero if the ζ th satellite is behind the horizon, f_ζ is the Doppler shift incurred by satellite motion (assumed to be constant over the considered timescales), and $\mathbf{a}_\zeta \in \mathbb{C}^B$ is the antenna arrangement steering vector (also assumed constant over the considered timescales), which is given as

$$\mathbf{a}_\zeta = \exp \left(-i2\pi \mathbf{O}^T \mathbf{v}(\theta_\zeta, \varphi_\zeta) / \lambda \right), \quad (3)$$

where the columns $\mathbf{o}_b = [x_b, y_b, z_b]^T$ of $\mathbf{O} = [\mathbf{o}_1, \dots, \mathbf{o}_B]$ contain the position coordinates of the receive antennas in a receiver-centric Cartesian coordinate system, and where $\mathbf{v}(\theta, \varphi) = [\cos \theta \cos \varphi, \cos \theta \sin \varphi, \sin \theta]^T$ is a unit vector pointing in the direction of the receive signal with elevation θ and azimuth φ (cf. Fig. 1), and λ is the signal wavelength.

The signal delay $\Delta t_\zeta = \tau_\zeta + \delta t$ is comprised of the path delay $\tau_\zeta = \|\mathbf{o}_\zeta - \mathbf{o}\|_2 / c$ (where c is the speed of light) and the receiver's internal clock offset δt from the global reference clock. This quantity represents the message delay perceived by the receiver with respect to its local clock sampling origin $k = 0$. For simplicity, we omit additional delay factors such as satellite-internal offsets or atmospheric influences.

As stated above, the receiver, the jammers, and the spoofers are assumed to be stationary, which is why the channels \mathbf{j}_j and \mathbf{q}_m do not depend on k . However, our methods are straightforwardly applicable also in situations where—like the satellites—these transceivers are moving with constant velocity. Moreover, we assume that the spoofers emulate satellite-like motion by modulating their transmit signals with virtual Doppler shifts (cf. Sec. II-B). We assume that the jammers and the spoofers either also exhibit LoS characteristics, in which case they have the form $\mathbf{j}_j = \alpha_j \mathbf{a}_j$ and $\mathbf{q}_m = \alpha_m \mathbf{a}_m$ with steering vectors as defined in (3), or that they exhibit independent identically distributed (i.i.d.) Rayleigh fading characteristics.

The ς th satellite's unit-power transmit signal is

$$t_\varsigma[k] = d_\varsigma[\lfloor k/L_c \rfloor] c_\varsigma[k \bmod L_c] \quad (4)$$

and consists of the product of the satellite's spreading code $\mathbf{c}_\varsigma = [c_\varsigma[0]; \dots; c_\varsigma[L_c - 1]]$ and its data symbols $d_\varsigma[\cdot]$. In real-world GNSS systems, these data symbols contain information about the current time, the satellite trajectory, satellite clock corrections, and more. In this work, however, we assume that the receiver knows the current time up to the timing error δt and has an offline almanac available, which allows it to estimate the current position \mathbf{o}_ς of each satellite (this is called a warm start [16]) without relying on the data symbols $d_\varsigma[\cdot]$. Hence, the only function of the data symbols is to impart the receiver with information about the path delay. To this end, we assume the data symbols to be given as

$$d_\varsigma[K] = \begin{cases} -1 & K < K_0 \\ +1 & K \geq K_0 \end{cases} \quad (5)$$

for some publicly known instant K_0 , which can be seen as a simplified model of a message header.

B. Attack Model

We distinguish between two types of interference:

Jamming describes interference consisting of noise-like random symbols. Throughout this work, when considering single-jammer attack scenarios, we model the jammer transmit symbols as zero-mean, i.i.d. complex random variables (also known as barrage jamming)

$$w[k] \sim \mathcal{CN}(0, N_J). \quad (6)$$

When considering distributed or multi-antenna jammer scenarios, we model the jammers as dynamically beamforming jammers, which are more challenging to mitigate than jammers that use constant beamforming [29]. For jammers with a total of I_J transmit antennas, the jammer transmit vectors are modeled as

$$\mathbf{w}[k] = \mathbf{B}[k] \mathbf{b}[k] \quad (7)$$

$$\mathbf{B}[k+1] = \begin{cases} \mathbf{B}[k] & \text{w.p. } 95\% \\ \Pi \text{diag}(\mathbf{1}_R^T, \mathbf{0}_{I_J-R}^T) & \text{w.p. } 5\%, \end{cases} \quad (8)$$

where $\mathbf{b}[\cdot] \stackrel{\text{i.i.d.}}{\sim} \mathcal{CN}(\mathbf{0}, \sigma_J^2 \mathbf{I}_{I_J})$ are jamming symbol vectors and Π is a random permutation matrix. Essentially the jamming symbols are beamformed using a matrix $\mathbf{B} \in \mathbb{C}^{B \times I_J}$ which activates R jamming antennas simultaneously, deciding randomly which R of the I_J antennas to use. We note, however, that the specific transmission model of the jammers is not critical for the efficacy of our mitigation method (e.g., non-Gaussian transmit signals would also be mitigated). The only relevant assumption is that the jammer transmit signals are random and independent of the satellite signals.

Spoofing, in contrast, is used to describe the intentional imitation of spreading codes or full satellite signals. While aimless, intermittent imitation of spreading codes without the transmission of sensible data symbols as in (4) can disrupt the regular acquisition approach, the subsequent decoding either produces insensible data or fails outright. In contrast,

the imitation of entire satellite data streams, either through replaying received signals (meaconing) or through emulation of satellite behavior, is harder to recognize and reject from positioning. We therefore consider smart spoofers that actually transmit satellite-like data symbols as in (5). Hence, the transmit signal of a spoofer $m \in \{1, \dots, I_M\}$ is¹

$$\check{t}_m[k] = \check{a}_m \sum_{\varsigma' \in \zeta_m} \check{d}_{\varsigma'}[k + \delta t_{\varsigma'}] c_{\varsigma'}[k + \delta t_{\varsigma'}] e^{i2\pi f_{\varsigma'} k T}. \quad (9)$$

Here, the spoofer imitates satellites from an index set ζ_m which contains the indices of $n_S = |\zeta_m|$ satellites to be spoofed. The data symbols $\check{d}_{\varsigma'}[\cdot] \in \mathbb{C}$ produce a credible message and are spread with the corresponding spreading codes of the mimicked satellites. A spoofer emulates the Doppler effect $f_{\varsigma'}$ as attackers are stationary in our model, and it introduces an individual delay $\delta t_{\varsigma'}$ for each spoofed satellite. This allows an adversary to create believable constellation streams in the receiver (apart from the different DoAs, which cannot be emulated by a single spoofer). Finally, \check{a}_m is a parameter for controlling the spoofer's signal power. Spoofing attacks attempting to cancel the original signal (i.e., to null it at the receiver) [30] require targeting and are extremely challenging to execute. Such an approach would require precise knowledge of the receiver's position, the attacker's distance to the receiver, and must match the original channel's features such that it is hardly feasible to implement against multi-antenna receivers. Thus, we have chosen not to consider it in our attacker model.

C. GNSS Prerequisites

We now provide a quick outline of regular GNSS positioning (i.e., GNSS positioning in the absence of jamming and spoofing) for a multi-antenna receiver that will serve as background for our method in Sec. III, and as the baseline for our evaluation in Sec. IV. We distinguish three stages: signal acquisition, pseudorange estimation, and positioning.

1) *Signal Acquisition*: Even in the absence of jamming and spoofing (i.e., when $I_J = I_M = 0$), the receive signal in (1) contains the time-delayed superposition of many satellite signals, all of which are considerably below the noise floor. When acquiring the ς th satellite's signal, the receiver searches for the code phase $\ell_\varsigma \triangleq \left\lfloor \frac{\Delta t_\varsigma}{T} \right\rfloor \bmod L_c$ (as viewed from the receiver) of the spreading code as well as the corresponding Doppler shift f_ς ; see (2). To this end, the receiver uses the ς th cross-ambiguity function (CAF) [16] which, for our multi-antenna receiver, we define as

$$\Xi_\varsigma[\ell, f] = \frac{\left\| \sum_{k=0}^{L_c-1} \mathbf{y}[k + \ell] c_\varsigma^*[k] e^{-i2\pi f k T} \right\|_2^2}{\sum_{k=0}^{L_c-1} \left\| \mathbf{y}[k + \ell] \right\|_2^2} \quad (10)$$

$$= \frac{\left\| \mathbf{Y}[\ell] \mathbb{D}(f) c_\varsigma^* \right\|_2^2}{\left\| \mathbf{Y}[\ell] \right\|_F^2}, \quad (11)$$

where

$$\mathbf{Y}[\ell] \triangleq [\mathbf{y}[\ell], \dots, \mathbf{y}[\ell + L_c - 1]] \quad (12)$$

¹In contrast to jamming, our spoofer transmit model does distinguish between single spoofer scenario and multi-spoofers scenarios.

is the windowed receive signal and

$$\mathbb{D}(f) = \text{diag}(1, e^{-i2\pi fT}, \dots, e^{-i2\pi f(L_c-1)T}) \quad (13)$$

is a diagonal matrix to compensate the Doppler shift. The ς th CAF measures the Doppler-adjusted and energy-normalized correlation of the windowed receive signal with the ς th satellite's spreading code \mathbf{c}_ς .² For the acquisition of the ς th satellite's signal, the receiver searches for the maximum of the CAF over all possible code phases $\ell \in \{1, \dots, L_c\}$ as well as over a quantized grid of potential Doppler shift compensations $f \in \mathcal{F}$:

$$(\hat{\ell}_\varsigma, \hat{f}_\varsigma) = \arg \max_{\substack{\ell \in \{1, \dots, L_c\} \\ f \in \mathcal{F}}} \{ \Xi_\varsigma[\ell, f] \mid \Xi_\varsigma[\ell, f] \geq \tau \}. \quad (14)$$

Note that, to prevent bogus acquisitions of Earth-obstructed satellites, the receiver only acquires a signal if the maximum of the CAF exceeds some threshold τ .

2) *Pseudorange Estimation*: When a signal has been acquired at phase $\hat{\ell}_\varsigma$ and Doppler shift \hat{f}_ς , it is despread using a replica of the ς th satellite's spreading code \mathbf{c}_ς , resulting in the symbol vector \mathbf{r}_ς . Defining the windowed transmit signal $\mathbf{t}_\varsigma^T[\ell] = [t_\varsigma[\ell], \dots, t_\varsigma[\ell + L_c - 1]]$, and assuming a perfect match of the acquired Doppler shift $\hat{f}_\varsigma = f_\varsigma$ and code phase $\hat{\ell}_\varsigma \equiv \left\lfloor \frac{\Delta t_\varsigma}{T} \right\rfloor \bmod L_c$, the K th symbol vector is computed as

$$\begin{aligned} \mathbf{r}_\varsigma[K] &\triangleq \mathbf{Y}[KL_c + \hat{\ell}_\varsigma] \mathbb{D}(\hat{f}_\varsigma) \mathbf{c}_\varsigma^* \\ &= \alpha_\varsigma \mathbf{a}_\varsigma \mathbf{t}_\varsigma^T \left[KL_c + \hat{\ell}_\varsigma - \left\lfloor \frac{\Delta t_\varsigma}{T} \right\rfloor \right] \mathbf{c}_\varsigma^* \\ &\quad \triangleq \Delta K_\varsigma L_c \\ &\quad + \sum_{\varsigma' \neq \varsigma} \alpha_{\varsigma'} \mathbf{a}_{\varsigma'} \mathbb{D}(\hat{f}_{\varsigma'} - f_{\varsigma'}) \mathbf{t}_{\varsigma'}^T \left[KL_c + \hat{\ell}_{\varsigma'} - \left\lfloor \frac{\Delta t_{\varsigma'}}{T} \right\rfloor \right] \mathbf{c}_{\varsigma'}^* \\ &\quad + \underbrace{\mathbf{N} \mathbb{D}(\hat{f}_\varsigma) \mathbf{c}_\varsigma^*}_{\triangleq \tilde{\mathbf{n}}} \end{aligned} \quad (15)$$

$$= \alpha_\varsigma \mathbf{a}_\varsigma \mathbf{t}_\varsigma^T [(K - \Delta K_\varsigma) L_c] \mathbf{c}_\varsigma^* + \tilde{\mathbf{n}} \quad (17)$$

$$= \alpha_\varsigma \mathbf{a}_\varsigma d_\varsigma [K - \Delta K_\varsigma] \|\mathbf{c}_\varsigma\|^2 + \tilde{\mathbf{n}} \quad (18)$$

where ΔK is the data index retardation by which the satellite's despread data symbol $D_\varsigma[\cdot]$ appears delayed due to the path delay, where $\tilde{\mathbf{n}} \in \mathbb{C}^B$ subsumes residual disturbance from the other satellite signals and thermal noise, where (17) follows from the fact that $\hat{\ell}_\varsigma \equiv \left\lfloor \frac{\Delta t_\varsigma}{T} \right\rfloor \bmod L_c$, and where (18) follows from (4). Since the other spreading codes $\mathbf{c}_{\varsigma'}$ are only weakly correlated with \mathbf{c}_ς regardless of whether or not they are cyclically shifted, the residual disturbance terms from the other satellites in (16) are significantly attenuated compared to the despread signal from the ς th satellite.

Note that \mathbf{a}_ς is not known at the receiver because the receiver knows neither its current position nor its orientation. However, the receiver can estimate the data retardation ΔK from the symbol vector sequence $\mathbf{r}_\varsigma[\cdot]$ by searching for the \hat{K}_ς , for

²In principle, the length over which the CAF measures the correlation may differ from the length of the spreading code. For simplicity, however, we assume these two lengths to be equal.

which $\mathbf{r}_\varsigma[\hat{K}_\varsigma]$ exhibits the phase change corresponding to K_0 in (5), and estimating $\Delta \hat{K}_\varsigma = \hat{K}_\varsigma - K_0$. Using the estimated data retardation $\Delta \hat{K}_\varsigma$ and the code phase $\hat{\ell}_\varsigma$, the receiver can then estimate the sum of the path delay and its internal time offset $\Delta t_j = \tau_\varsigma + \delta t$ as $(\hat{\ell}_\varsigma + L_c \Delta \hat{K}_\varsigma)T$. Multiplication with the speed of light c gives the so-called *pseudorange* estimate

$$\hat{R}_\varsigma \triangleq c(\hat{\ell}_\varsigma + L_c \Delta \hat{K}_\varsigma)T. \quad (19)$$

3) *Positioning*: Barring non-idealities, the “true” pseudorange R_ς is a function of the coordinates $\mathbf{o}_\varsigma = [x_\varsigma, y_\varsigma, z_\varsigma]^T$ and $\mathbf{o} = [x, y, z]^T$ of the ς th satellite and the receiver, respectively. The pseudorange is then given as

$$R_\varsigma = \underbrace{\|\mathbf{o}_\varsigma - \mathbf{o}\|_2}_{\triangleq \rho(\mathbf{o}_\varsigma, \mathbf{o})} + c \delta t. \quad (20)$$

That is, R_ς is a function of the four unknown variables x, y, z , and $c \delta t$ and the four known variables x_ς, y_ς , and z_ς . Denote the set of satellites ς whose pseudoranges have been successfully acquired by \mathcal{S} , then the receiver position can be inferred (provided that $|\mathcal{S}| \geq 4$) by solving the least squares problem

$$\min_{\mathbf{o}, c \delta t} \sum_{\varsigma \in \mathcal{S}} \left(\hat{R}_\varsigma - \rho(\mathbf{o}_\varsigma, \mathbf{o}) - c \delta t \right)^2, \quad (21)$$

where \hat{R}_ς is the estimate of R_ς from (19). A difficulty lies in the nonlinearity of $\rho(\mathbf{o}_\varsigma, \mathbf{o})$, which is commonly addressed by using an iterative approach in which $\rho(\mathbf{o}_\varsigma, \mathbf{o})$ is linearized at every iteration [2, Sec. 2.5.2]: if $\mathbf{o}^{(k)}$ is the estimated receiver position at iteration k , then the first-order Taylor approximation of $\rho(\mathbf{o}_\varsigma, \mathbf{o})$ at $\mathbf{o}^{(k)}$ is as follows:

$$\begin{aligned} \rho(\mathbf{o}_\varsigma, \mathbf{o}) &\approx \rho(\mathbf{o}_\varsigma, \mathbf{o}^{(k)}) + \frac{x^{(k)} - x_\varsigma}{\rho(\mathbf{o}_\varsigma, \mathbf{o}^{(k)})} (x - x^{(k)}) \\ &\quad + \frac{y^{(k)} - y_\varsigma}{\rho(\mathbf{o}_\varsigma, \mathbf{o}^{(k)})} (y - y^{(k)}) + \frac{z^{(k)} - z_\varsigma}{\rho(\mathbf{o}_\varsigma, \mathbf{o}^{(k)})} (z - z^{(k)}). \end{aligned} \quad (22)$$

Thus, defining $\rho_\varsigma^{(k)} \triangleq \rho(\mathbf{o}_\varsigma, \mathbf{o}^{(k)})$, $\delta^{(k)} \triangleq [\hat{R}_\varsigma - \rho_\varsigma^{(k)}]_{\varsigma \in \mathcal{S}} \in \mathbb{R}^{|\mathcal{S}|}$, and the matrix

$$\mathbf{A}^{(k)} \triangleq \begin{bmatrix} \frac{x^{(k)} - x_\varsigma}{\rho_\varsigma^{(k)}} & \frac{y^{(k)} - y_\varsigma}{\rho_\varsigma^{(k)}} & \frac{z^{(k)} - z_\varsigma}{\rho_\varsigma^{(k)}} & 1 \end{bmatrix}_{\varsigma \in \mathcal{S}} \in \mathbb{R}^{|\mathcal{S}| \times 4}, \quad (23)$$

the problem (21) can be approximately solved via iterations

$$\begin{bmatrix} \mathbf{o} \\ c \delta t \end{bmatrix}^{(k+1)} = \arg \min_{\mathbf{o}, c \delta t} \left\| \delta^{(k)} + \mathbf{A}^{(k)} \begin{bmatrix} \mathbf{o}^{(k)} \\ 0 \end{bmatrix} - \mathbf{A}^{(k)} \begin{bmatrix} \mathbf{o} \\ c \delta t \end{bmatrix} \right\|^2 \quad (24)$$

$$= \begin{bmatrix} \mathbf{o}^{(k)} \\ 0 \end{bmatrix} + \left(\mathbf{A}^{(k)} \right)^\dagger \delta^{(k)}, \quad (25)$$

where $\mathbf{o}^{(k_{\max})}$ gives the estimate of the receiver coordinates. A typical initialization is the Earth's center $\mathbf{o}^{(0)} = [0, 0, 0]^T$ [31].

III. JAMMER AND SPOOFER MITIGATION

Jammers and spoofers interfere with the traditional GNSS receiver from Sec. II-C in different ways: Jammers try to impede the signal acquisition and/or pseudorange estimation entirely, while spoofers try to induce erroneous pseudoranges at the receiver based on spuriously acquired signals. We therefore

mitigate jammers at the signal acquisition stage (Sec. III-A), whereas spoofed signals are identified and rejected during the pseudorange estimation stage (Sec. III-B). Moreover, to increase the robustness of positioning in case that a spoofer manages to bypass the spoofer rejection stage, we use an outlier-resistant position estimation procedure (Sec. III-C).

A. Jammer-Resistant Signal Acquisition

The goal of our modified (compared to Sec. II-C1) signal acquisition is to determine the presence, phase, and Doppler shift of satellite signals in the receive signal even under jammer interference. Signals from other satellites appear as (weak) noise after despreading with \mathbf{c}_ζ (see (16) and also Fig. 2(a)). Jamming signals likewise appear as noise; but because of their much larger energy, this noise tends to drown the desired signal (see Fig. 2(c)).³ However, what distinguishes the noise due to jammer interference is that it is confined to a rank- I_J subspace of the receive signal space [29], so that adaptive spatial filtering can be used to identify and null the interference subspace.

To this end, we leverage JASS [7], a recently developed method for jammer-resilient time synchronization, with which we enhance the signal acquisition described in Sec. II-C1: Consider the projection matrix

$$\mathbf{T}_\zeta \triangleq \mathbf{I}_{L_c} - \mathbf{c}_\zeta^* \mathbf{c}_\zeta^T / \|\mathbf{c}_\zeta\|_2^2, \quad (26)$$

which projects (in the time domain) a signal onto the orthogonal complement of the subspace spanned by the spreading code \mathbf{c}_ζ^T . This property can be leveraged for separating the ζ th satellite's signal of interest from interfering signals by projecting the windowed and Doppler-compensated (for the candidate Doppler shift f) receive signal $\mathbf{Y}[\ell] \mathbb{D}(f)$ (see (12) and (13)) onto said subspace:

$$\tilde{\mathbf{Y}}_\zeta(\ell, f) \triangleq \mathbf{Y}[\ell] \mathbb{D}(f) \mathbf{T}_\zeta. \quad (27)$$

If the sample window is correctly aligned to a signal present in the receive samples using this spreading code (i.e., if $\ell = \ell_\zeta$) and if the candidate Doppler compensation matches the true Doppler shift (i.e., if $f = f_\zeta$), then the projection \mathbf{T}_ζ eliminates the ζ th satellite's transmit signal. The resulting matrix $\tilde{\mathbf{Y}}_\zeta$ therefore consists entirely of interfering signals (from jammers as well as other satellites) and noise. The dominant \hat{I} spatial dimensions⁴ of this interference can be identified by performing an eigenvalue decomposition of the matrix $\tilde{\mathbf{Y}}_\zeta(\ell, f) \tilde{\mathbf{Y}}_\zeta(\ell, f)^H$,

$$\tilde{\mathbf{Y}}_\zeta(\ell, f) \tilde{\mathbf{Y}}_\zeta(\ell, f)^H = [\mathbf{E}_{\hat{I}} \quad \mathbf{E}_n] \begin{bmatrix} \mathbb{D}_{\hat{I}} & \mathbf{0} \\ \mathbf{0} & \mathbb{D}_n \end{bmatrix} \begin{bmatrix} \mathbf{E}_{\hat{I}}^H \\ \mathbf{E}_n^H \end{bmatrix}, \quad (28)$$

where $\mathbb{D}_{\hat{I}} \in \mathbb{R}_{\geq 0}^{\hat{I} \times \hat{I}}$ is a diagonal matrix that contains the \hat{I} largest eigenvalues of $\tilde{\mathbf{Y}}_\zeta(\ell, f) \tilde{\mathbf{Y}}_\zeta(\ell, f)^H$ and $\mathbf{E}_{\hat{I}} \in \mathbb{C}^{B \times \hat{I}}$ contains the corresponding orthonormal eigenvectors. We identify the image of $\mathbf{E}_{\hat{I}}$ with the estimated interference subspace, and the image of \mathbf{E}_n with the estimated noise

³Spoofers signals appear as additional peaks in the CAF if the spoofer spoofs the ζ th satellite (see Fig. 2(d)) and as noise akin to the signals from the other satellites otherwise.

⁴The number of jammers I_J would presumably be unknown in practice, so \hat{I} corresponds to an estimate thereof. Overestimating I_J is not critical, but underestimating it is, see [7] and the experiments in Sec. IV.

subspace. The interference subspace can now be nulled using the orthogonal projection

$$\tilde{\mathbf{P}} = \mathbf{I}_B - \mathbf{E}_{\hat{I}} \mathbf{E}_{\hat{I}}^\dagger, \quad (29)$$

which projects (in the spatial domain) a signal onto the orthogonal complement of the image of $\mathbf{E}_{\hat{I}}$.

Following JASS [7], we now modify the regular CAF from (11) to include the interference-nulling projection from (29):

$$\tilde{\Xi}_\zeta[\ell, f] \triangleq \frac{\|\tilde{\mathbf{P}} \mathbf{Y}[\ell] \mathbb{D}(f) \mathbf{c}_\zeta^*\|_2^2}{\|\tilde{\mathbf{P}} \mathbf{Y}[\ell]\|_F^2}. \quad (30)$$

As in the traditional acquisition in (14), we now try to acquire the ζ th satellite's signal by searching over all possible code phases and Doppler shifts. A naïve way of doing this would be to replace $\Xi_\zeta[\ell, f]$ in (14) with $\tilde{\Xi}_\zeta[\ell, f]$ from (30). However, if we only extract the (single) maximizing argument, we risk that a spoofer which spoofs the ζ th satellite's signal would create a second CAF peak that is higher than the legitimate one (cf. Fig. 2(d)), in which case only the spoofed signal would be acquired. To circumvent this issue, we acquire *all* signals corresponding to a CAF peak, which enables us to identify and reject spoofed signals later on (see Sec. III-B). To this end, we determine the set of signals satisfying

$$\mathcal{V}_\zeta \triangleq \left\{ (\ell, f) \in \{1, \dots, L_c\} \times \mathcal{F} \mid \tilde{\Xi}_\zeta[\ell, f] \geq \tau_J \text{ and } \tilde{\Xi}_\zeta[\ell, f] \text{ is a local maximum} \right\}. \quad (31)$$

Note that $|\mathcal{V}_\zeta| > 1$ is a clear indication that the ζ th satellite is being spoofed.

We define the total set of all acquired signals as

$$\mathcal{V} \triangleq \bigcup_{\zeta=1}^S \mathcal{V}_\zeta, \quad (32)$$

and we use $\zeta(\nu)$ for $\nu \in \mathcal{V}$ to denote the index of the satellite which matches the signal ν (i.e., $\nu \in \mathcal{V}_{\zeta(\nu)}$ for all $\nu \in \mathcal{V}$). For every acquired signal $\nu \in \mathcal{V}$, the receiver then estimates the corresponding pseudorange $\hat{R}_{\zeta(\nu)}$ as in (19).

B. Spoofer-Resistant Pseudorange Estimation

The goal of our modified (compared to Sec. II-C2) pseudorange estimation is to identify which of the signals acquired in Sec. III-A correspond to spoofers in order to reject them and only end up with pseudorange estimates of legitimate satellites.

To this end, we first estimate the DoA of all acquired signals. We then develop a novel approach that tests the consistency of pairs of signals by comparing their respective DoAs and pseudoranges with the almanac *without* any knowledge of the receiver's position. Finally, using these pairwise consistency tests, we try to identify the set of legitimate signals.

1) *Direction of Arrival Estimation:* For each acquired signal $\nu \in \mathcal{V}$, let $(\hat{\ell}_\nu, \hat{f}_\nu) = \nu$ denote the corresponding code phase and Doppler estimate (cf. (31)), and let $\tilde{\mathbf{P}}_\nu$ denote the corresponding projection matrix from (29). We now despread the receive signal as in the traditional GNSS receiver in

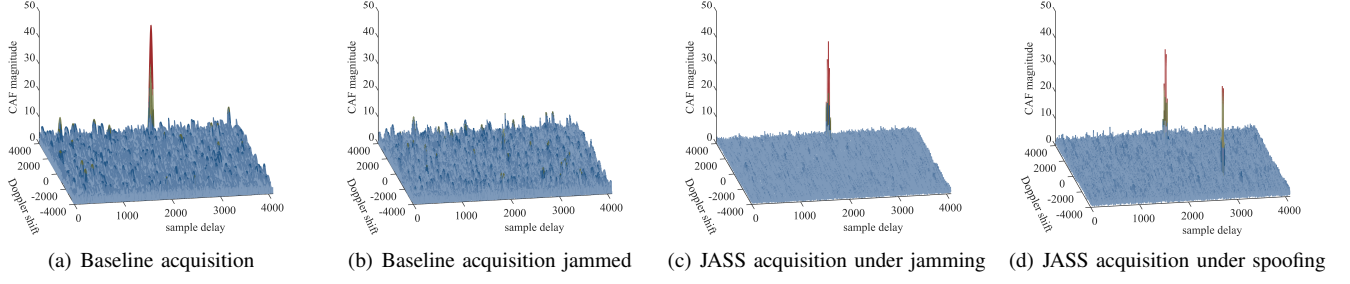


Fig. 2. Illustration of the traditional CAF $\Xi_\zeta[\ell, f]$ without Fig. 2(a)) and with jamming (Fig. 2(b)), as well as of the jammer-resilient CAF $\tilde{\Xi}_\zeta[\ell, f]$ with jamming (Fig. 2(c)) and with spoofing (Fig. 2(d)). The figures are for the L1 C/A PRN 2 code, sampled at four times the chiprate ($L_c = 4092$). Fig. 2(a) shows a receiver with $B = 8$ antennas at $SNR = -20$ dB (cf. Sec. IV-A for definitions of SNR and JSR) in absence of jamming. In Fig. 2(b), a single-antenna barrage jammer with $JSR = 30$ dB is active and obfuscates the satellite signal, such that the traditional acquisition fails. Fig. 2(c) shows the same situation, but for the jammer resistant acquisition from Sec. III-A (with $\hat{I} = 4$), which not only null-steers jamming but also improves the noise floor. Fig. 2(d) shows that jammer-resistant acquisition remains vulnerable to spoofing, since a spoofer with $SSR = 0$ dB in this example causes a second, equally high, peak in the CAFs.

Sec. II-C2, but adding in the jammer-mitigating projection $\tilde{\mathbf{P}}_\nu$. Assuming the accuracy of $\hat{\ell}_\nu$ and \hat{f}_ν , we obtain

$$\mathbf{r}_\nu[K] = \tilde{\mathbf{P}}_\nu \mathbf{Y}[KL_c + \ell_\nu] \mathbb{D}(\hat{f}_\nu) \mathbf{c}_{\zeta(\nu)}^* \quad (33)$$

$$= \tilde{\mathbf{P}}_\nu (\alpha_\zeta \mathbf{a}_\zeta d_\zeta[K - \Delta K_\zeta] \|\mathbf{c}_\zeta\|^2 + \tilde{\mathbf{n}}), \quad (34)$$

where $\tilde{\mathbf{n}}$ subsumes residual disturbance from the other satellite signals and thermal noise, as well as any residual jamming interference. Estimating the signal's DoA is tantamount to estimating the steering vector \mathbf{a}_ζ ; see (3). To this end, we use a modified version of the MUSIC algorithm that takes into account the spatial filter $\tilde{\mathbf{P}}_\nu$'s influence on the receive signal. As in the traditional MUSIC algorithm [8], we collect a window $\mathbf{R}_\nu = [\mathbf{r}_\nu[K], \dots, \mathbf{r}_\nu[K + Z - 1]] \in \mathbb{C}^{B \times Z}$ of receive vectors from which we compute the empirical spatial covariance matrix of $\mathbf{r}_\nu[\cdot]$ as $\frac{1}{Z} \mathbf{R}_\nu \mathbf{R}_\nu^H$. We then perform an eigenvalue decomposition of the empirical covariance matrix,

$$\frac{1}{Z} \mathbf{R}_\nu \mathbf{R}_\nu^H = [\mathbf{e}_1 \quad \mathbf{E}_N] \begin{bmatrix} \sigma_1 & \mathbf{0} \\ \mathbf{0} & \mathbb{D}_N \end{bmatrix} \begin{bmatrix} \mathbf{e}_1^H \\ \mathbf{E}_N^H \end{bmatrix}, \quad (35)$$

where σ_1 is the principal eigenvalue with corresponding eigenvector \mathbf{e}_1 , and where $\mathbf{E}_N \in \mathbb{C}^{B \times (B-1)}$ contains the eigenvectors corresponding to the remaining eigenvalues.

To estimate the DoA, we consider a grid of testing angles $\theta \in \Theta \subset [0, \pi/2]$ and $\varphi \in \Phi \subset [-\pi, \pi]$ with corresponding steering vectors $\mathbf{a}(\theta, \varphi)$ as in (3). To take into account the fact that the spatial filter $\tilde{\mathbf{P}}_\nu$ nulls signals from certain directions, we estimate the DoA of the signal $\nu \in \mathcal{V}$ as follows:

$$(\hat{\theta}_\nu, \hat{\varphi}_\nu) = \arg \min_{(\theta, \varphi) \in \Theta \times \Phi} \left\| \mathbf{E}_N^H \frac{\tilde{\mathbf{P}}_\nu \mathbf{a}(\theta, \varphi)}{\|\tilde{\mathbf{P}}_\nu \mathbf{a}(\theta, \varphi)\|} \right\|^2 \quad (36)$$

$$= \arg \max_{(\theta, \varphi) \in \Theta \times \Phi} \frac{\|\tilde{\mathbf{P}}_\nu \mathbf{a}(\theta, \varphi)\|^2}{\|\mathbf{E}_N^H \tilde{\mathbf{P}}_\nu \mathbf{a}(\theta, \varphi)\|^2}, \quad (37)$$

and we define the objective in (37) to be zero if $\tilde{\mathbf{P}}_\nu \mathbf{a}(\theta, \varphi) = \mathbf{0}$. The corresponding steering vector is denoted $\hat{\mathbf{a}}_\nu \triangleq \mathbf{a}(\hat{\theta}_\nu, \hat{\varphi}_\nu)$.

This DoA estimation approach builds upon the idea that the acquired signal ν impinges under LoS conditions, which we assumed was the case for unobstructed satellite signals. However, we assumed that spoofed signals could impinge under Rayleigh fading conditions as well as LoS conditions (cf.

Sec. II-A). If the objective value of the maximizing argument of (37) is small, then it indicates that the impinging signal does not exhibit LoS conditions, which—given our assumptions—can be used as a preliminary indicator for identifying spoofed signals. Hence, we reject all signals $\nu \in \mathcal{V}$ for which the maximal objective value in (37) is smaller than some threshold τ_M , and we denote the remaining set of signals by $\check{\mathcal{V}}$.

2) *Pairwise Consistency Test*: We now introduce a novel approach to test the consistency of pairs of signals by comparing their respective DoAs and pseudoranges with the almanac *without* knowing the receiver's position. Assume for the moment that both ν and $\nu' \in \check{\mathcal{V}}$ correspond to legitimate signals from two different satellites $\zeta(\nu)$ and $\zeta(\nu')$, respectively. We therefore consider the difference between the known (from the almanac) positions $\mathbf{o}_{\zeta(\nu)}$ and $\mathbf{o}_{\zeta(\nu')}$ of the satellites $\zeta(\nu)$ and $\zeta(\nu')$, which can be written as

$$\mathbf{o}_{\zeta(\nu)} - \mathbf{o}_{\zeta(\nu')} = \mathbf{o} + \rho_{\zeta(\nu)} \mathbf{Q} \mathbf{v}_{\zeta(\nu)} - (\mathbf{o} + \rho_{\zeta(\nu')} \mathbf{Q} \mathbf{v}_{\zeta(\nu')}) \quad (38)$$

$$= \mathbf{Q} (\rho_{\zeta(\nu)} \mathbf{v}_{\zeta(\nu)} - \rho_{\zeta(\nu')} \mathbf{v}_{\zeta(\nu')}), \quad (39)$$

where \mathbf{o} is the receiver's (as of yet) unknown position in ECEF coordinates, \mathbf{Q} is the unknown rotation matrix which rotates the receiver-centered antenna coordinate system of the antenna arrangement (Fig. 1) into the ECEF coordinate system at the receiver position, and $\mathbf{v}_{\zeta(\nu)} \triangleq \mathbf{v}(\theta_{\zeta(\nu)}, \varphi_{\zeta(\nu)})$ and $\mathbf{v}_{\zeta(\nu')} \triangleq \mathbf{v}(\theta_{\zeta(\nu')}, \varphi_{\zeta(\nu')})$ are the unitary direction vectors (cf. the right-hand-side in (3)) towards the satellites $\zeta(\nu)$ and $\zeta(\nu')$, respectively. We now take the squared norm of (38) and obtain

$$\|\mathbf{o}_{\zeta(\nu)} - \mathbf{o}_{\zeta(\nu')}\|^2 = \|\rho_{\zeta(\nu)} \mathbf{v}_{\zeta(\nu)} - \rho_{\zeta(\nu')} \mathbf{v}_{\zeta(\nu')}\|^2 \quad (40)$$

$$= \rho_{\zeta(\nu)}^2 \|\mathbf{v}_{\zeta(\nu)}\|^2 - 2\rho_{\zeta(\nu)} \rho_{\zeta(\nu')} \mathbf{v}_{\zeta(\nu)}^T \mathbf{v}_{\zeta(\nu')} + \rho_{\zeta(\nu')}^2 \|\mathbf{v}_{\zeta(\nu')}\|^2 \quad (41)$$

$$= (\rho_{\zeta(\nu)} - \rho_{\zeta(\nu')})^2 + 2\rho_{\zeta(\nu)} \rho_{\zeta(\nu')} - 2\rho_{\zeta(\nu)} \rho_{\zeta(\nu')} \mathbf{v}_{\zeta(\nu)}^T \mathbf{v}_{\zeta(\nu')}, \quad (42)$$

where (42) follows from the fact that $\mathbf{v}_{\zeta(\nu)}$ and $\mathbf{v}_{\zeta(\nu')}$ are unit vectors, and by completing the square. Following the pseudorange relation from (20), we can now rewrite the range

difference $\rho_{\varsigma(\nu)} - \rho_{\varsigma(\nu')}$ in (42) as follows:

$$\rho_{\varsigma(\nu)} - \rho_{\varsigma(\nu')} = \rho_{\varsigma(\nu)} + c \delta t - \rho_{\varsigma(\nu')} - c \delta t \quad (43)$$

$$= R_{\varsigma(\nu)} - R_{\varsigma(\nu')} \quad (44)$$

$$\triangleq \Delta_R. \quad (45)$$

Rearranging (45) into $\rho_{\varsigma(\nu')} = \rho_{\varsigma(\nu)} - \Delta_R$ and plugging this into (42) yields the quadratic equation

$$\|\mathbf{o}_{\varsigma(\nu)} - \mathbf{o}_{\varsigma(\nu')}\|^2 = \Delta_R^2 + 2\rho_{\varsigma(\nu)}(\rho_{\varsigma(\nu)} - \Delta_R)(1 - \mathbf{v}_{\varsigma(\nu)}^T \mathbf{v}_{\varsigma(\nu')}). \quad (46)$$

Note that the receiver can compute the value of the left-hand-side from the almanac, that it can obtain an estimate of Δ_R by computing $\hat{\Delta}_R = \hat{R}_{\varsigma(\nu)} - \hat{R}_{\varsigma(\nu')}$ (where $\hat{R}_{\varsigma(\nu)}$ and $\hat{R}_{\varsigma(\nu')}$ have been estimated in Sec. III-A), and that it has obtained estimates of $\mathbf{v}_{\varsigma(\nu)}$ and $\mathbf{v}_{\varsigma(\nu')}$ in Sec. III-B1. Hence, by plugging in these estimates, the receiver can obtain an estimate for the unknown range $\rho_{\varsigma(\nu)}$ using the quadratic formula⁵

$$\hat{\rho}_{\nu \leftarrow \nu'} = \frac{-b + \sqrt{b^2 - 4ac}}{2a}, \quad (47)$$

where

$$a = 2(1 - \hat{\mathbf{v}}_{\varsigma(\nu)}^T \hat{\mathbf{v}}_{\varsigma(\nu')}) \quad (48)$$

$$b = -2\hat{\Delta}_R(1 - \hat{\mathbf{v}}_{\varsigma(\nu)}^T \hat{\mathbf{v}}_{\varsigma(\nu')}) \quad (49)$$

$$c = \hat{\Delta}_R^2 - \|\mathbf{o}_{\varsigma(\nu)} - \mathbf{o}_{\varsigma(\nu')}\|^2. \quad (50)$$

Remember that the derivation of (47) (from (38) on) was based on the premise that both ν and ν' correspond to legitimate signals from satellites $\varsigma(\nu)$ and $\varsigma(\nu')$. If this premise is violated, (47) tends to give bogus results because the direction vectors $\hat{\mathbf{v}}_{\varsigma(\nu)}$ and $\hat{\mathbf{v}}_{\varsigma(\nu')}$ are inconsistent with the almanac positions $\mathbf{o}_{\varsigma(\nu)}$ and $\mathbf{o}_{\varsigma(\nu')}$ in (38) (when the spoofer does not successfully replicate the satellite geometry), or because the difference of estimated pseudoranges $\hat{\Delta}_R$ is inconsistent with the range difference in (45) (when the spoofer does not successfully replicate the satellite's timing at the receiver).

We now use this behavior to our advantage: Given the GNSS satellite orbits, for any location \mathbf{o} on Earth and for any satellite ς , the range $\rho_{\varsigma} = \|\mathbf{o}_{\varsigma} - \mathbf{o}\|_2$ should be within some range $[\rho_{\min}, \rho_{\max}]$. Moreover, from the triangle inequality, it follows that c in (50) should be negative. If one or both of these conditions are violated, this is indicative that either ν or ν' may not correspond to a legitimate satellite signal. For any two signals ν and ν' , we therefore define the following plausibility function:

$$p(\nu, \nu') = \begin{cases} 1 & \text{if } \hat{\rho}_{\nu \leftarrow \nu'} \in [\rho_{\min}, \rho_{\max}] \text{ and } c < 0 \\ 0 & \text{else.} \end{cases} \quad (51)$$

Using this function, we can generate the plausibility matrix $\mathbf{G} \in \{0, 1\}^{|\mathcal{V}| \times |\mathcal{V}|}$ whose entries are given by $p(\nu, \nu')$, $\nu, \nu' \in \mathcal{V}$. Note that $p(\nu, \nu') \neq p(\nu', \nu)$ because $\hat{\rho}_{\nu \leftarrow \nu'} \neq \hat{\rho}_{\nu' \leftarrow \nu}$, and so \mathbf{G} is not symmetric. However, we can get a symmetric plausibility matrix \mathbf{G}_{sym} from \mathbf{G} as

$$\mathbf{G}_{\text{sym}} = \mathbf{G} \odot \mathbf{G}^T. \quad (52)$$

⁵The subscript $\nu \leftarrow \nu'$ indicates that the range of the satellite corresponding to signal ν was estimated using the signal ν' as a reference

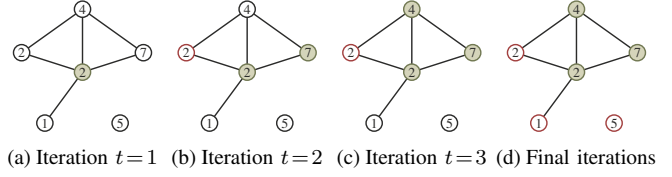


Fig. 3. Illustration of the greedy clique finding algorithm of (53). In the first iteration, the vertex of maximum degree is added to the clique (shown in green), whose satellite index is $\varsigma = 2$. In the second iteration, another signal with satellite index $\varsigma = 2$ is passed over (shown in red), and the tie between the $\varsigma = 4$ and $\varsigma = 7$ signals is arbitrarily broken in favor of the latter. In the third iteration, the $\varsigma = 4$ signal is added to the clique. In the remaining iterations, there are no vertices that can be added to the clique and the algorithm terminates accordingly.

This matrix can be interpreted as the adjacency matrix of an undirected graph $\mathcal{G} = (\mathcal{V}, \mathcal{E})$ whose vertices are the acquired signals \mathcal{V} . Two signals ν and ν' are connected within \mathcal{G} if and only if $p(\nu, \nu')p(\nu', \nu) = 1$, i.e., if the relative range estimates $\hat{\rho}_{\nu \leftarrow \nu'}$ and $\hat{\rho}_{\nu' \leftarrow \nu}$ are both plausible according to (51).

3) *Identifying the Set of Legitimate Signals:* A complete subgraph of \mathcal{G} corresponds to a set of signals that are all consistent with each other in the sense of satisfying the plausibility function in (51). We therefore try to infer the set of legitimate signals by searching for the largest complete subgraph of \mathcal{G} , i.e., for the maximum clique in \mathcal{G} [32]. However, finding the maximum clique of a graph is an NP-hard problem [32], so we use an approximate method based on a greedy approach.

We first search for the vertex with the highest degree, with which we initialize the clique: $\text{clique}^{(0)} = \arg \max_{\nu \in \mathcal{V}} \deg(\nu)$.⁶ We then iteratively augment the clique with the vertex that has the highest degree among all remaining vertices which (i) is connected with all nodes that are already included in the clique, and which (ii) does not correspond to a satellite that is already represented in the clique (since each satellite can have at most one legitimate signal):

$$\text{clique}^{(t+1)} = \text{clique}^{(t)} \cup \arg \max_{\substack{\nu \in \mathcal{V} \\ \forall \nu' \in \text{clique}^{(t)}: (\nu, \nu') \in \mathcal{E} \\ \forall \nu' \in \text{clique}^{(t)}: \varsigma(\nu) \neq \varsigma(\nu')}} \deg(\nu). \quad (53)$$

We denote the set of signals included in the final clique (i.e., the signals deemed to be legitimate) as $\check{\mathcal{V}}$. An explanatory illustration of this algorithm is provided in Fig. 3. The numbers in the vertices designate the satellite ID in the tuple and the operation is illustrated from left to right.

C. Outlier-Resistant Positioning

The plausibility filtering yields a clique of tuples which are spatially consistent with one another within the constellation's dimensional relations. Spoofed signals that closely match the DoA of the corresponding legitimate signal but that are marginally shifted in terms of the pseudorange can potentially bypass the spoofer rejection. For this reason, we modify the position estimation method to make it resistant to outliers.

The set of selected signals $\check{\mathcal{V}}$ corresponds to the pseudorange estimates $\hat{R}_{\varsigma(\nu)}$, $\nu \in \check{\mathcal{V}}$ and satellite positions $\mathbf{o}_{\varsigma(\nu)}$, $\nu \in \check{\mathcal{V}}$

⁶If there are multiple maximizing vertices, we select one of them at random. The same holds for (53).

required to estimate the position of the receiver. Instead of iteratively solving the linearized least-squares problems (24), which give each acquired pseudorange ς the same weight, we use an IRLS approach [33] in which the different pseudorange estimates $\hat{R}_{\varsigma(\nu)}, \nu \in \check{\mathcal{V}}$ are weighted with an iteration-dependent weighting matrix $\mathbf{W}^{(k)} = \text{diag}(w_1^{(k)}, \dots, w_{|\check{\mathcal{S}}|}^{(k)})$. That is, instead of iterating (24), we iterate

$$\begin{aligned} & \begin{bmatrix} \mathbf{o} \\ c \delta t \end{bmatrix}^{(k+1)} \\ &= \arg \min_{\mathbf{o}, c \delta t} \left\| \left(\mathbf{W}^{(k)} \right)^{\frac{1}{2}} \left(\boldsymbol{\delta}^{(k)} + \mathbf{A}^{(k)} \begin{bmatrix} \mathbf{o}^{(k)} \\ 0 \end{bmatrix} - \mathbf{A}^{(k)} \begin{bmatrix} \mathbf{o} \\ c \delta t \end{bmatrix} \right) \right\|^2 \end{aligned} \quad (54)$$

$$= \begin{bmatrix} \mathbf{o}^{(k)} \\ 0 \end{bmatrix} + ((\mathbf{A}^{(k)})^T \mathbf{W}^{(k)} \mathbf{A}^{(k)})^{-1} (\mathbf{A}^{(k)})^T \mathbf{W}^{(k)} \boldsymbol{\delta}^{(k)}, \quad (55)$$

where $\boldsymbol{\delta}^{(k)} \triangleq [\hat{R}_{\varsigma(\nu)} - \rho_{\varsigma(\nu)}^{(k)}]_{\nu \in \check{\mathcal{V}}} \in \mathbb{R}^{|\check{\mathcal{V}}|}$ with $\rho_{\varsigma(\nu)}^{(k)} \triangleq \rho(\mathbf{o}_{\varsigma(\nu)}, \mathbf{o}^{(k)})$, and where diagonal entries $w_{\varsigma(\nu)}^{(k)} > 0$ of the weighting matrix $\mathbf{W}^{(k)}$ correspond to the reliabilities of the respective acquired pseudoranges. These reliabilities are iteratively computed from the data as

$$w_{\varsigma}^{(k+1)} = \left(\frac{1}{\max\{\sigma, e_{\varsigma(\nu)}^{(k+1)}\}} \right)^2, \quad (56)$$

where

$$\begin{aligned} & \mathbf{e}^{(k+1)} \\ &= \boldsymbol{\delta}^{(k)} + \mathbf{A}^{(k)} \begin{bmatrix} \mathbf{o}^{(k)} \\ 0 \end{bmatrix} - \mathbf{A}^{(k)} \begin{bmatrix} \mathbf{o} \\ c \delta t \end{bmatrix}^{(k+1)} \end{aligned} \quad (57)$$

$$= (\mathbf{I}_{|\check{\mathcal{V}}|} - \mathbf{A}^{(k)} ((\mathbf{A}^{(k)})^T \mathbf{W}^{(k)} \mathbf{A}^{(k)})^{-1} (\mathbf{A}^{(k)})^T \mathbf{W}^{(k)}) \boldsymbol{\delta}^{(k)}, \quad (58)$$

and where $\sigma = \frac{1}{6} cT$ represents the intrinsic imprecision of the acquired pseudoranges.⁷

IV. EVALUATION IN SIMULATION

A. Simulation Setup

We now evaluate the efficacy of SCHIEBER using MATLAB simulations. Our simulator models the physical constellation of GPS satellites, a receiver positioned on Earth, and the GPS L1 C/A signals arriving onto its antenna arrangement. Within this framework, the influence of different attack scenarios on positioning is assessed. The satellite positions are initialized at the reference epoch positions [34], from where we simulate their trajectories along their ideal trajectories up to the timestamp of simulation. For simplicity of the simulation, we assume circular orbits without perturbations. We assume that the receiver is positioned on the surface of the Earth, which we model as a perfect sphere. For every satellite in the GPS constellation, we deduce the satellite visibility (or lack thereof) above the receiver's horizon. For every visible satellite, we compute the distance, velocity towards the receiver, and the

DoAs of the incoming signal at the receiver. From these values the signal properties for each receivable satellite follow from our model in Sec. II-A, which yields the satellite signal part of (1).

We model the satellite signal attenuation using a simple distance-based model: the mean distance ρ_0 of a LoS satellite ($\rho_0 \approx 23'000$ km) is normalized such that it corresponds to a channel gain of $\|\mathbf{h}_0\|^2 = B$ after channel attenuation as in (2). All other distance-induced attenuations are scaled according to their distance with respect to this mean distance ρ_0 using the free-space path loss model

$$\|\mathbf{h}_{\varsigma}\| = \|\mathbf{h}_0\| \frac{\rho_0}{\rho_{\varsigma}}. \quad (59)$$

The noise power is specified in terms of the mean received signal-to-noise ratio (SNR) using the mean satellite path gain $\|\mathbf{h}_0\|^2$:

$$SNR = \frac{\mathbb{E} [\|\mathbf{h}_0 t_{\varsigma}[\cdot]\|^2]}{\mathbb{E} [\|\mathbf{n}[k]\|^2]} = \frac{B}{\mathbb{E} [\|\mathbf{n}[k]\|^2]}. \quad (60)$$

Both for SCHIEBER and for the performance baseline, the receiver is equipped with $B = 8$ antennas that are arranged in a ring, with neighboring antennas being separated by half a wavelength. In the simulations, the receiver remains stationary such that the satellite Doppler frequency range is ± 4 kHz. The signals are sampled at four times their chiprate, i.e., at 4.092 MHz.⁸ The acquisition is performed over a single spreading code of length $L_c = 4092$ and over a Doppler granularity of $\delta f = 250$ Hz. We empirically set the acquisition threshold for the baseline and for SCHIEBER to $\tau = 11.2$ and $\tau_J = 7.5$, respectively. The jammer-resistant acquisition rejects an interference subspace of dimension $\hat{I} = 4$. For the DoA estimation, we use a window of $Z = 10$ consecutive vectors, over which the DoA of all impinging LoS signals is assumed to remain constant. The DoA search is performed over the sets $\Theta = \{0^\circ, 1^\circ, \dots, 90^\circ\}$ and $\Phi = \{0^\circ, 1^\circ, \dots, 359^\circ\}$, and we empirically set the LoS threshold to $\tau_M = 10$. The plausibility range for the distance estimation in (47) is set to $[\rho_{\min}, \rho_{\max}] = [18'000\text{km}, 28'000\text{km}]$, which allows for some margin of error (the real distance between an Earth-surface receiver and a GPS satellite above the horizon is in the range of 20'000 km to 27'000 km).

As performance metric, we consider the empirical cumulative distribution function (CDF) of the Euclidean distance between the actual position and the projection of the estimated position onto the Earth's surface. Each empirical CDF is computed from 200 Monte-Carlo trials. For every trial, the satellites are placed at the reference epoch positions [34] for a randomly drawn time within the year 2024; the receiver is placed uniformly at random on the Earth's surface, and jammers as well as spoofers are placed randomly anywhere in the hemisphere above the receiver's horizon. Unless noted otherwise, attack signals are assumed to impinge onto the receive antenna array under pure LoS conditions. When noted otherwise, we assume i.i.d. Rayleigh fading, i.e., we draw the attacker channels \mathbf{j}_j

⁷This value for σ is obtained by assuming that the pseudorange measurement error is uniformly distributed on the interval $[-0.5 cT, +0.5 cT]$, and thus has standard deviation proportional to cT . The factor $1/6$ is chosen empirically.

⁸Reference [35] discourages whole integer oversampling due to precision loss caused by the chip duration uncertainty. Our design choice is motivated by simplified front-end simulation at the cost of higher positioning errors, which would allow future works to improve this aspect.

and \mathbf{q}_m from $\mathcal{CN}(\mathbf{0}, \mathbf{I}_B)$.

B. Interference Signals

Single and multi-antenna jammers operate as described in Sec. II-B, so the jammer transmit signals are

$$\mathbf{w}[k] = \begin{cases} w[k] \sim \mathcal{CN}(0, \sigma_J^2) & I_J = 1 \\ \mathbf{B}[k]\mathbf{b}[k], \mathbf{b}[k] \sim \mathcal{CN}(\mathbf{0}, \sigma_J^2 \mathbf{I}_R) & I_J \geq 2, \end{cases} \quad (61)$$

where the beamforming matrix $\mathbf{B}[k]$ is defined as described in (8), and where R is set to $R = B - 1$ (i.e., for multi-antenna jamming, a randomly chosen jamming antenna is inactive at any point in time). A jammer's interference power is characterized relative to the mean received satellite signal power in terms of the per-transmit-antenna jammer-to-signal ratio (JSR)

$$JSR = \frac{\mathbb{E} [\|\mathbf{j}_j w_j[k]\|_2^2]}{\mathbb{E} [\|\mathbf{h}_0 s[k]\|_2^2]}. \quad (62)$$

In our simulation, spoofers only try to impersonate satellites that are visible to the receiver. Spoofers start replicating true satellite signals *before* the receiver starts with signal acquisition, i.e., like satellites, spoofers are active for the entire simulation duration. They imitate complete satellite messages even though the actual content is irrelevant in the simulations as long as the pseudorange is measurable. The spoofing power is characterized relative to the mean received satellite signal power in form of the per-transmit-signal (cf. (9)) spoofer-to-signal ratio (SSR)

$$SSR = \frac{\frac{1}{n_s} \mathbb{E} [\|\mathbf{q}_m \tilde{t}_m[k]\|_2^2]}{\mathbb{E} [\|\mathbf{h}_0 s[k]\|_2^2]}. \quad (63)$$

In all spoofer scenarios, each spoofer antenna imitates the same number n_s of satellites. We set the delay of the spoofed signals such that they appear at somewhat realistic distance to the receiver in comparison to the legitimate signals. These distances are randomly selected in the range of 20 000 km to 29 000 km for each imitated signal. The Doppler frequency of each spoofed satellite signal is randomly selected in the range of ± 4 kHz, not necessarily mirroring the Doppler shift of the imitated satellite since SCHIEBER makes no plausibility interpretation of the estimated Doppler shift.

C. Results

1) *Performance in Jammer-Free, Spoofer-Free GPS:* We start by comparing the positioning performance of SCHIEBER and the baseline in the absence of jamming and spoofing. Fig. 4 shows empirical CDFs of the positioning error for different SNRs. For an SNR of -20 dB or higher, SCHIEBER and the baseline have virtually identical performance, with a positioning error of 30 m or less.⁹ At lower SNRs, SCHIEBER outperforms the baseline even in the absence of spoofing or jamming. The reason for this is due to the fact that jammer-resistant signal acquisition stage of SCHIEBER (cf. Sec. III-A) also helps to mitigate the mutual interference of the GPS

⁹Note that the positioning error of commercial GPS receivers in the L1 band is typically around 2.5 m [36]. This performance difference is explained by our simplified receiver architecture, which uses integer oversampling [35] and does not perform smoothing of the estimated position over time. Improving both of these aspects is left for future work.

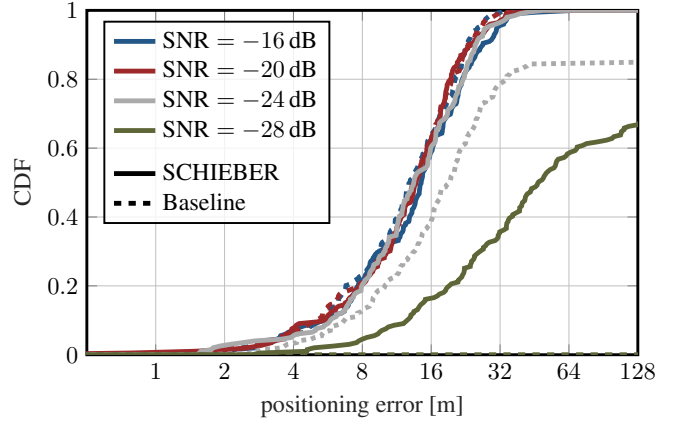


Fig. 4. Cumulative distribution function (CDF) of the positioning error of SCHIEBER and the corresponding baseline in the absence of jamming or spoofing.

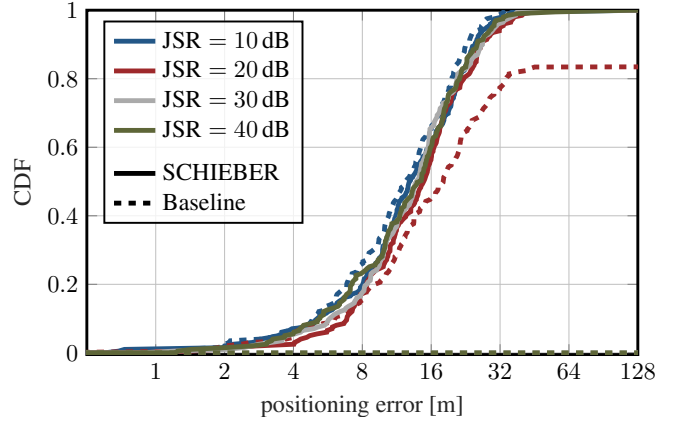


Fig. 5. Cumulative distribution function (CDF) of the positioning error of SCHIEBER and the corresponding baseline in the under jamming by a single-antenna jammer, for different jamming-to-signal ratios (JSRs).

satellites. Note that -24 dB and -28 dB are the respective SNRs at which the baseline and SCHIEBER occasionally fail to acquire enough satellite signals for successful positioning, which can lead to positioning errors in the order of tens of thousands of kilometers.

2) *Performance Against Jamming:* Next, we consider the performance against jammers. Fig. 5 shows the performance against one single-antenna jammer with different jamming powers at an SNR of -20 dB. At a JSR of 10 dB, the received jammer power is negligible comparable to the noise power, so the baseline achieves comparable positioning performance as in the interference-free case (cf. Fig. 4). However, at a JSR of 20 dB, the jammer interference becomes noticeable, and the baseline fails to achieve positioning in around 20% of cases. For JSRs of 30 dB or more, the jammer interference becomes critical, and the baseline fails completely. However, thanks to the jammer-mitigating signal acquisition (cf. Sec. III-A), SCHIEBER achieves comparable performance as in the interference-free case regardless of the jammer power. In particular, SCHIEBER achieves a positioning error of around 30 m or less in all cases.

Fig. 6 shows the performance against multiple jammers

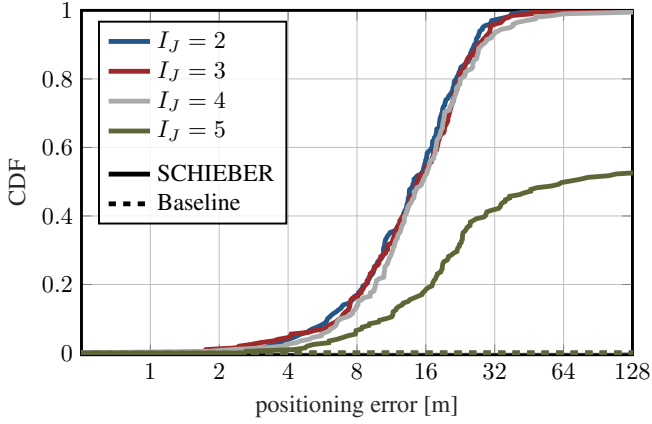


Fig. 6. Cumulative distribution function (CDF) of the positioning error of SCHIEBER and the corresponding baseline in the under jamming by a multi-antenna jammer, for different numbers of jammer antennas.

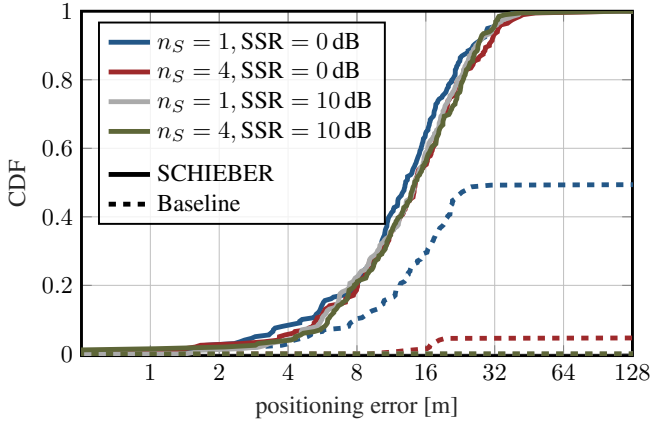


Fig. 7. Cumulative distribution function (CDF) of the positioning error of SCHIEBER and the corresponding baseline in the under spoofing by a single spoofer, for different spoofer-to-signal ratios (SSRs) and different numbers of spoofed satellites n_S .

(ranging from $I_J = 2$ to $I_J = 5$) at a JSR of 30 dB and an SNR of -20 dB. At these jammer powers, the baseline fails completely regardless of the number of jammers. In contrast, SCHIEBER, whose jammer-mitigating signal acquisition nulls an interference-subspace of dimension $\hat{I} = 4$ (cf. Sec. IV-A), successfully mitigates the jammers as long as $I_J \leq \hat{I} = 4$. In these cases, the positioning performance matches the performance of the interference-free case (cf. Fig. 4). However, $I_J = 5$ exceeds the dimension \hat{I} of the nulled interference-subspace, so that SCHIEBER mitigates the interference only partially, and positioning fails in around 50% of the cases.

3) *Spoofing*: We now turn to analyzing the performance against spoofers. Fig. 7 shows the performance (at SNR = -20 dB) against one single-antenna spoofer that simultaneously spoofs the signal of $n_S = 1$ or $n_S = 4$ satellites at JSR = 0 dB or JSR = 10 dB. If the spoofer only spoofs a single satellite at JSR = 0 dB, it is based purely on luck whether the baseline receiver acquires the legitimate signal or the spoofed signal. Hence, the baseline fails in 50% of the cases. However, if the spoofer power increases to JSR = 10 dB, the baseline receiver consistently acquires the spoofed signal and thus

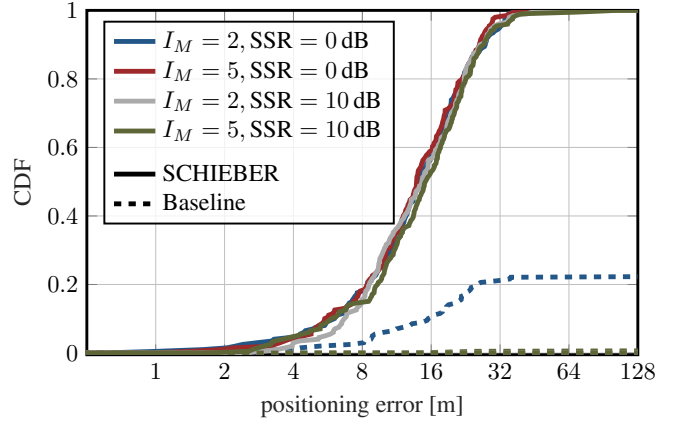


Fig. 8. Cumulative distribution function (CDF) of the positioning error of SCHIEBER and the corresponding baseline in the under spoofing by a multiple spoofers, for different spoofer-to-signal ratios (SSRs) and different numbers of spoofers I_M .

fails completely. If the spoofer spoofs $n_S = 4$ satellites at SSR = 0 dB, there is a roughly $1 - 0.5^4 = 0.9375$ probability that the baseline receiver acquires at least one spoofed signal instead of the corresponding legitimate signal. Hence, the baseline achieves successful positioning in less than 10% of the cases. And if the spoofer power increases to SSR = 10 dB, the baseline again fails completely. In contrast, thanks to the spoofer-resistant pseudorange estimation (cf. Sec. III-B), SCHIEBER is able to reject the spoofed signals and achieve positioning with comparable performance as in the unspoofed case.

Fig. 8 shows the performance (at SNR = -20 dB) against multiple spoofers, where each spoofer spoofs the signal of one satellite, either at SSR = 0 dB or at SSR = 10 dB. For the case of $I_M = 2$ with SSR = 0 dB, it is again based purely on luck whether the baseline receiver acquires the legitimate signals or the spoofed signals. Hence, there is a 25% probability of acquiring the legitimate rather than the spoofed signals in both cases, as reflected by the 25% success rate of positioning. In all other cases, the baseline exhibits only negligible chances of correct positioning. In contrast, SCHIEBER is again able to reliably reject the spoofed signals and to achieve positioning with comparable performance as in the unobstructed case.

4) *Simultaneous Jamming and Spoofing*: Finally, we consider the performance against simultaneous jamming and spoofing. Moreover, in this experiment, we also consider what happens when the attackers' channels exhibit i.i.d. Rayleigh fading rather than LoS characteristics. Fig. 9 shows the performance (at SNR = -20 dB) against $I_J = 2$ jammers with a JSR of 30 dB and $I_M = 2$ spoofers with an SSR of 10 dB. The results show that in both cases, the baseline fails completely while SCHIEBER is able to mitigate the jammers as well as the spoofers, and still achieves the same performance as in the unobstructed case.

V. CONCLUSIONS

We have proposed SCHIEBER, a novel multi-antenna based method for resilient GNSS positioning under both multi-antenna jamming and multi-antenna spoofing. Compared to

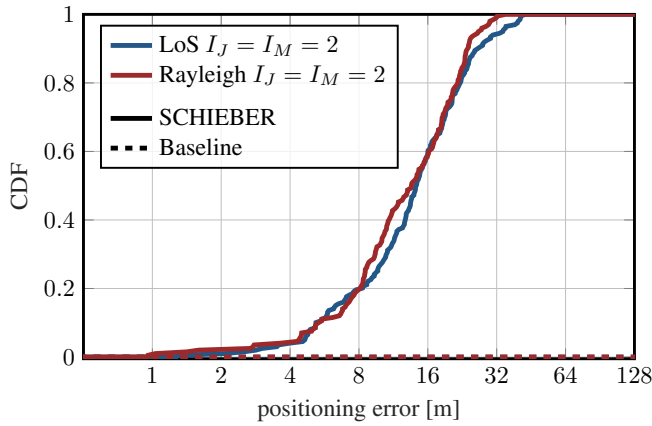


Fig. 9. Cumulative distribution function (CDF) of the positioning error of SCHIEBER and the corresponding baseline in the under simultaneous jamming and spoofing.

traditional GNSS receivers, SCHIEBER uses a modified signal acquisition stage that mitigates jammers based on adaptive spatial filtering. SCHIEBER then rejects spoofed signals based on a novel receiver-position-invariant pairwise plausibility test. The efficacy of SCHIEBER is demonstrated via extensive systems simulation and for a range of different attack scenarios.

The main advantages of SCHIEBER compared to the state of the art is that it makes minimal assumptions about the attackers (in particular, the number and type of attackers need not be known, no assumptions about the receive power of the attackers' signals are made, and the channels of the attackers can be LoS as well as Rayleigh fading) and that it requires *no* a priori estimate of the receiver position. Limitations to be addressed in future work are the assumption of a pure LoS link between the receiver and the legitimate satellites as well as the limited positioning precision due to integer oversampling and the absence of tracking and smoothing over time.

REFERENCES

- [1] EUSPA. (2024, Jul.) EUSPA, EO and GNSS Market Report, Issue 2. [Online]. Available: https://www.euspa.europa.eu/sites/default/files/external/publications/euspa_market_report_2024.pdf
- [2] E. D. Kaplan and C. J. Hegarty, *Understanding GPS/GNSS, Principles and Applications, Third Edition*. Artech House, 2017.
- [3] Z. Wu, Y. Zhang, Y. Yang, C. Liang, and R. Liu, "Spoofing and Anti-Spoofing Technologies of Global Navigation Satellite System: A Survey," *IEEE Access*, vol. 8, pp. 165 444–165 496, 2020.
- [4] P. Papadimitratos and A. Jovanovic, "GNSS-based positioning: attacks and countermeasures," in *Procs. IEEE Military Commun. Conf. (MILCOM)*, Nov. 2008, pp. 1–7.
- [5] I. Fernández-Hernández, V. Rijmen, G. Seco-Granados, J. Simon, I. Rodríguez, and J. D. Calle, "A navigation message authentication proposal for the Galileo open service," *NAVIGATION*, vol. 63, no. 1, pp. 85–102, 2016.
- [6] EUSPA. (2024, Nov.) Galileo is getting ready for the upcoming OSNMA operational declaration. [Online]. Available: <https://www.euspa.europa.eu/pressroom/trending-topics/galileo-getting-ready-upcoming-osnma-operational-declaration>
- [7] G. Marti, F. Arquint, and C. Studer, "Jammer-resilient time synchronization in the MIMO uplink," *IEEE Trans. Signal Process.*, vol. 73, pp. 706–720, 2025.
- [8] R. Schmidt, "Multiple emitter location and signal parameter estimation," *IEEE Trans. Antennas Propag.*, vol. 34, no. 3, pp. 276–280, Mar. 1986.
- [9] National Coordination Office for Space-Based Positioning. (2024, Aug.) IRN-IS-200M-001. Aug 2022, Rev N. [Online]. Available: <https://www.gps.gov/technical/icwg/IS-GPS-200N.pdf>
- [10] C. J. Hegarty, "GNSS Signals-An Overview," in *Procs. IEEE Int. Frequency Contr. Symp.*, May 2012, pp. 1–7.
- [11] L. Milstein, "Interference rejection techniques in spread spectrum communications," *Procs. IEEE*, vol. 76, no. 6, pp. 657–671, Jun. 1988.
- [12] D. Borio and C. Gioia, "GNSS interference mitigation: A measurement and position domain assessment," *NAVIGATION*, vol. 68, no. 1, pp. 93–114, 2021.
- [13] R. Wu, W. Wang, D. Lu, L. Wang, and Q. Jia, *Adaptive Interference Mitigation in GNSS*. Springer, 2018.
- [14] M. Amin and W. Sun, "A novel interference suppression scheme for global navigation satellite systems using antenna array," *IEEE J. Sel. Areas Commun.*, vol. 23, no. 5, pp. 999–1012, May 2005.
- [15] S. Daneshmand, A. Broumandan, J. Nielsen, and G. Lachapelle, "Interference and multipath mitigation utilising a two-stage beamformer for global navigation satellite systems applications," *IET Radar, Sonar & Navigation*, vol. 7, no. 1, pp. 55–66, 2013.
- [16] J. W. Betz, *Engineering Satellite-Based Navigation and Timing*. John Wiley & Sons, 2015.
- [17] A. Ranganathan, H. Ólafsson, and S. Capkun, "SPREE: a spoofing resistant GPS receiver," in *Procs. ACM Int. Conf. Mobile Comput. Netw. (MOBICOM)*, Oct. 2016, p. 348–360.
- [18] S. Han, L. Chen, W. Meng, and C. Li, "Improve the security of GNSS receivers through spoofing mitigation," *IEEE Access*, vol. 5, pp. 21 057–21 069, 2017.
- [19] Z. Gülgün, E. G. Larsson, and P. Papadimitratos, "Multiple Spoofing Detection for Mobile GNSS Receivers Using Statistical Tests," *IEEE Access*, vol. 9, pp. 166 382–166 394, 2021.
- [20] M. L. Psiaki, B. W. O'Hanlon, S. P. Powell, J. Bhatti, K. D. Wesson, T. E. Humphreys, and A. Schofield, "GNSS spoofing detection using two-antenna differential carrier phase," vol. 4, Jan. 2014, pp. 2776–2800.
- [21] F. Rothmaier, Y.-H. Chen, S. Lo, and T. Walter, "GNSS spoofing detection through spatial processing," *NAVIGATION*, vol. 68, no. 2, pp. 243–258, 2021.
- [22] Y. Zhao, F. Shen, D. Xu, and Z. Meng, "A coprime array-based technique for spoofing detection and DOA estimation in GNSS," *IEEE Sensors J.*, vol. 22, no. 23, pp. 22 828–22 835, Dec. 2022.
- [23] M. Meurer, A. Konovaltsev, M. Cuntz, and C. Hättich, "Robust joint multi-antenna spoofing detection and attitude estimation using direction assisted multiple hypotheses RAIM," in *Procs. Int. Tech. Meeting Satellite Division Inst. Navigation (ION GNSS)*, vol. 4, Sep. 2012, pp. 3007–3016.
- [24] R. Shi and C. Liu, "Detection on Satellite Navigation Deception Signals Based on Multi Platforms Cooperation," in *China Satellite Navigation Conference (CSNC) 2019 Proceedings*, J. Sun, C. Yang, and Y. Yang, Eds. Singapore: Springer Singapore, 2019, pp. 553–561.
- [25] Y. Hu, S. Bian, B. Li, and L. Zhou, "A novel array-based spoofing and jamming suppression method for GNSS receiver," *IEEE Sensors J.*, vol. 18, no. 7, pp. 2952–2958, Apr. 2018.
- [26] J. Zhang, X. Cui, H. Xu, and M. Lu, "A two-stage interference suppression scheme based on antenna array for GNSS jamming and spoofing," *Sensors*, vol. 19, no. 18, p. 3870, 2019.
- [27] Q. Yang, Y. Zhang, C. Tang, and J. Lian, "A combined antijamming and antispoofing algorithm for GPS arrays," *Int. J. Ant. Prop.*, vol. 2019, no. 1, p. 8012569, 2019.
- [28] S. Zorn, T. Bamberg, and M. Meurer, "Accurate position and attitude determination in a jammed or spoofed environment using an uncalibrated multi-antenna-system," in *Procs. Int. Tech. Meeting Inst. Navigation*, Jan. 2018, pp. 690–702.
- [29] G. Marti and C. Studer, "Universal MIMO jammer mitigation via secret temporal subspace embeddings," in *Proc. Asilomar Conf. Signals, Syst., Comput.*, Oct. 2023, pp. 1–8.
- [30] M. L. Psiaki and T. E. Humphreys, "GNSS spoofing and detection," *Procs. IEEE*, vol. 104, no. 6, pp. 1258–1270, Jun. 2016.
- [31] J. Sanz Subirana, J. M. Juan Zornoza, and M. Hernández-Pajares, *GNSS Data Processing, Vol I: Fundamentals and Algorithms*. ESA Communications, 2013.
- [32] R. M. Karp, "Reducibility among combinatorial problems," in *Complexity of Computer Computations*. Springer, 1972, pp. 85–103.
- [33] J. E. Gentle, *Matrix Algebra*. Springer, 2007.
- [34] National Coordination Office for Space-Based Positioning. (2024, Jul.) Global Positioning System, Standard Positioning Service Performance Standard. April 2020, 5th Edition. [Online]. Available: <https://www.gps.gov/technical/ps/2020-SPS-performance-standard.pdf>
- [35] D. M. Akos and M. Pini, "Effect of sampling frequency on GNSS receiver performance," *NAVIGATION*, vol. 53, no. 2, pp. 85–95, 2006.
- [36] u-blox. (2024, Nov.) NEO-M8, u-blox M8 concurrent GNSS modules, Data sheet. [Online]. Available: https://content.u-blox.com/sites/default/files/NEO-M8-FW3_DataSheet_UBX-15031086.pdf